The On-Ground Calibrations of SuperAGILE: I. X-ray Pencil Beam

Y. Evangelista*[a], E. Costa[a], E. Del Monte[a], G. Di Persio[a], I. Donnarumma[a], M. Feroci[a], M. Frutti[a], A. Generosi[b], I. Lapshov[a], F. Lazzarotto[a], M. Mastropietro[c], E. Morelli[d], L. Pacciani[a], G. Porrovecchio[a], M. Rapisarda[e], V. Rossi-Albertini[b], A. Rubini[a], G. Sabatino[a], P. Soffitta[a]

[a]INAF IASF Roma, Via Fosso del Cavaliere 100, I-00133 Roma, Italy
[b]ISM CNR, Via Fosso del Cavaliere 100, I-00133 Roma, Italy
[c]ISC CNR, Via Salaria km 29.300, I-00016 Monterotondo Scalo (RM), Italy
[d]INAF IASF Bologna, Via P. Gobetti 101, I-40129 Bologna, Italy
[e]ENEA C.R. Frascati, Via Enrico Fermi 45, I-00044 Frascati (RM), Italy

ABSTRACT

The Flight Model of the SuperAGILE experiment was calibrated on-ground using an X-ray generator and individual radioactive sources at IASF Rome on August 2005. Here we describe the set-up, the measurements and the preliminary results of the calibration session carried out with the X-ray generator. The calibration with omnidirectional radioactive sources are reported elsewhere. The beam was collimated using a two slits system in order to reach a rectangular spot at the detector approximately 1800 μm $\times$ 100 μm in size. The long dimension was aligned with the detector strip, so that the short dimension could fall within one single detector strip (121 μm wide). The detector was then slowly moved continuously such that the beam effectively scanned along the coding direction. This measurement was done both at detection plane level (i.e., without collimator and mask) to characterize the detector response, and at experiment level (i.e., with collimator, mask and digital electronics), to study the imaging response. Aim of this calibration is the measurement of the imaging response at 0, 10 and 20 degrees off-axis, with a parallel beam, although spatially limited to a $\sim$2 mm long section of the coded mask.

Keywords: AGILE mission, High Energy Astrophysics, X-ray monitor, Coded Mask, Calibration.

1. INTRODUCTION

SuperAGILE[1] (SA) is the hard X-ray monitor of the AGILE satellite mission, devoted to the High Energy Astrophysics in the 15 keV$\div$45 keV and 30 MeV$\div$50 GeV energy bands. AGILE is a mission of the Italian Space Agency (ASI) proposed, designed, built and operated by a scientific collaboration including INAF IASF institutes at Rome, Milano and Bologna, INFN divisions at Trieste and Rome ("La Sapienza" and "Tor Vergata"), CIFS (Torino and Rome), ENEA (Frascati and Bologna). Design, manufacturing and testing support was given to this team by the industrial teams at MIPOT (Gorizia), Alcatel Alenia Space (formerly Laben, Milan), Oerlikon Contraves (Rome), Carlo Gavazzi Space (Milan) and Telespazio (Rome).

The launch is planned in early 2007 on an equatorial low earth orbit with 560 km altitude and less than 10 degrees inclination. SuperAGILE is the first X-ray instrument based on the technology of the silicon microstrip detectors to be part of a space mission and is based on the coded aperture imaging technique. The SuperAGILE detection plane (Fig 1-a) is composed of four silicon microstrip detector modules (121 μm pitch), each one with 19 $\times$ 19 cm^2 area, 410 μm thickness and 1536 strips. The modules are mechanically coupled and aligned to corresponding tungsten one-dimensional coded mask modules, of the same area and 120 μm thickness. The detector strips are separately and individually connected to the input analogue channels of the front-end electronics, composed of 48 XAA1.2 ASIC low-power chips manufactured by Ideas ASA (Norway). Each of the four SuperAGILE units can produce 1-D images of the X-ray (15-45 keV) sky in a 107° $\times$ 68° field of view (FOV)

* Correspondence: Email: yuri.evangelista@iasf-roma.inaf.it; Telephone: +39-06-49934657; Fax: +39-06-20660188

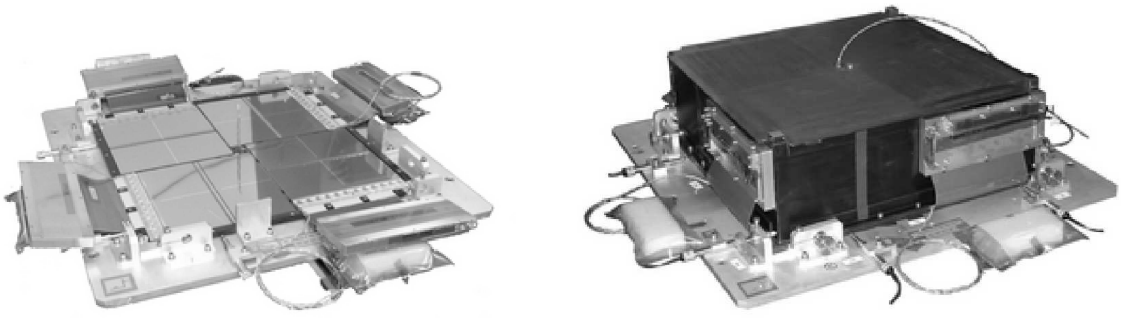

(a) (b)

Figure 1. (a) SuperAGILE detection plane composed by four silicon microstrip detectors and four independent front-end electronics modules (SAFEE). (b) Fully-integrated experiment. SAFEE are mounted on collimator walls in the final instrument configuration.

with 6 arcmin angular resolution, 3 arcmin sky pixel size and $1 \div 2$ arcmin positioning accuracy (for intense sources). The geometric configuration of silicon microstrip modules and masks permits to obtain orthogonal 1-D images of the sky in the central $68° \times 68°$ ($\sim$1 steradians) part of the FOV, with an on-axis sensitivity better $\sim$10 mCrab (5σ, 1 day). The main scientific objective of SA is the simultaneous observations in the X-ray band of the gamma-ray sources observed by AGILE above 30 MeV. However, its large FOV makes it very suitable for detecting and localizing hard X-ray transients, with particular care devoted to Gamma Ray Bursts (GRBs), that we expect to detect and localize at a rate of $\sim 10 \div 20$ GRBs/year. When triggered and localized on-board, their coordinates at $5 \div 10$ arcmin level will be automatically and freely distributed the worldwide observers within few minutes from the event through a dedicated link based on the ORBCOMM telecommunication network.

2. MEASUREMENT STRATEGY

In order to measure the detector efficiency, instrument effective area, Point Spread Function (PSF) and source location accuracy, the SuperAGILE flight model was calibrated both at detection plane level (i.e., without collimator and mask, Fig. 1-a) and at experiment level (i.e., with collimator and mask, Fig. 1-b) at IASF-Roma Laboratories using an X-ray generator. Figure 2 shows energy spectra from the X-ray tube measured with a

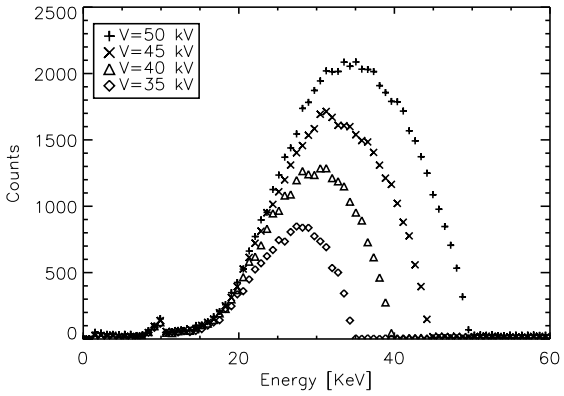

Figure 2. X-ray tube spectra measured with a Germanium detector for different HV values.

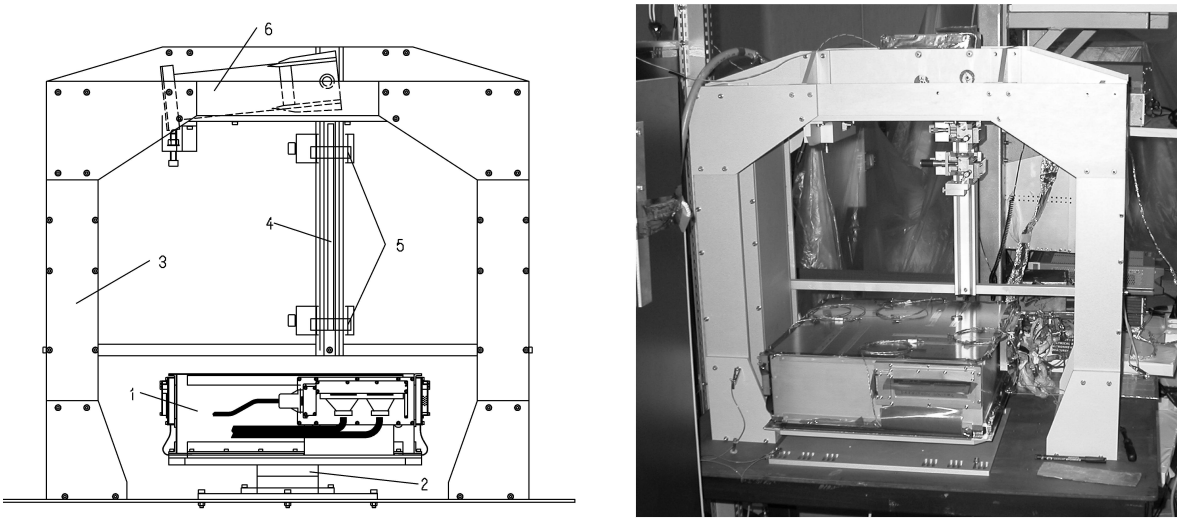

(a) (b)

Figure 3. Mechanical setup for SuperAGILE on-ground calibrations: 1 - SuperAGILE, 2 - Translational stage, 3 - Aluminium alloy structure, 4 - Slits holders and brass tube, 5 - Tungsten slits, 6 - X-ray tube.

Germanium detector for different settings of the high voltage. Our choice of HV = 45 kV was done to optimize the SuperAGILE energy band coverage.

The beam was collimated using a two tungsten slits system in order to obtain a rectangular spot at the detector plane with size of approximately 1800 μm (along microstrips) and 100 μm (perpendicular to microstrips). Using a motorized translational stage the detector was moved continuously at a constant speed of 60 μm$\cdot$s^{-1} along the coding direction, thus to irradiate the instrument with homogeneous intensity parallel beam. Temporal data analysis of detected photons allows to reconstruct the input beam position and study the space-resolved detector response during the calibration of the detection plane, particularly for what concerns the instrument effective area and inter-strip efficiency.

Similarly, during the calibration of the integrated experiment, the timing analysis allows to construct an effective parallel beam illumination of the experiment, emulating a source at infinite distance. In fact, the divergence of the beam is $\sim$0.7 arcmin, to be compared to the 3 arcmin pixel size, allowing to separate the beam divergence contribution to the PSF. Our set-up allows to perform this measurement at positions close to 0°, 10° and 20° with respect to the optical axis of the experiment. These measurements have one major limitation: the beam spot is small and only illuminates a fraction of the physical mask, with its specific mechanical properties and focal distance. Thus, these measurements need to be complemented with global measurements of the mask response. We performed this type of calibration using radioactive sources at distance of approximately 2 meters. The description of these measurements and the methods for the correction of the beam divergence are provided in Donnarumma et al.[2]

3. EXPERIMENTAL SETUP

The requirement for the X-ray pencil beam calibration was to have a stable and controlled scan of the detector with the X-ray beam. Considering the weight, volume (including the HV supply and water-cooling system) and the required accuracy of the two-slit system, the choice was made to have the beam facility steady, and move the SA detector and experiment underneath. To achieve this, a bridge-like mechanical structure was designed (Fig. 3-a) and built (Fig. 3-b) to support the beam above the SA experiment, in turn mounted on a motorized,

PC-controlled translational stage. Due to the absence of collimator and mask during first calibration runs, a collimator-like aluminium box (Fig. 3-b) was used in the aim of supporting the SAFEE electronics, of protecting silicon detectors and front-end electronics from dust, light and damages.

Anode material	Tungsten (W)	**Focus Dimensions***	0.4×8 mm^2
Power (Max.)	2.0 kW	**HV (Max.)**	60 kV
Window Material	Beryllium (Be)	**Emission Current (Max.)**	60 mA
Window Thickness	300 μm	**Cooling**	Water (closed system)

*Projected focal spot dimensions on the Be window, at 6 degrees take-off angle.

Table 1. Characteristics of the X-ray tube Panalytical PW2214/20.

The X-ray tube used for this calibration is a water cooled fixed tungsten anode *Panalytical* XRD glass tube (mod. PW2214/20), with 2.0 kW max power and 60 kV (High Voltage max.) 60 mA (Emission Current max.) and it was situated about 60 cm away from the SuperAGILE detection plane. The main characteristics of the X-ray generator are summarized in Tab. 1. Power supply was provided by *Ital Structures* Compact 3K5 HV generator. Declared instability is ±0.1 kV (HV) and ±0.1 mA (Emission Current) with ±10% maximum mains voltage variations. X-ray tube axis was inclined of 84 degrees with respect to SuperAGILE "optical" axis, thus to reach maximum beam intensity and stability as suggested by the manufacturer. The beam produced by the X-ray tube was collimated using two tungsten rectangular slits placed 5 cm and 45 cm away from the beryllium window with dimensions of 2000 μm × 140 μm (for the slit closer to beryllium window) and 640 μm × 20 μm (for the other slit). The slits were connected by a lead covered brass tube in order to avoid X-ray Compton scattering by aluminium slits holders and stray light. The spot at the detector was then as narrow as ∼100 μm, that is fully included in one single detector strip.

The detector movement was provided by a PC controlled translational stage (mod. M410-CG) equipped with a stepper motor and an incremental encoder, interfaced with SuperAGILE tray by an aluminium plate 10 mm thickness. This linear stage, produced by *Physik Instrumente* (PI), guarantees 0.1 μm minimum incremental motion, 2 μm repeatability and 100 mm travel range. Control software was entirely developed in C++ language using PI provided Dynamic Link Library (DLL) while motion drive was implemented by a PCI dedicated board.

In the two calibration set-up (detection plane and integrated experiment), the SuperAGILE Front-End Electronics (SAFEE) configuration and data acquisition was provided by two different test-equipments (TE)[3] developed by our group. SAFEE-TE was used to perform detection plane calibration, since interface electronic boards (SAIE, SuperAGILE Interface Electronics) had not completed their stand-alone acceptance tests at the time of this calibration campaign, whereas experiment-level calibration was executed using the flight units of the SAIE boards and harness, read-out through the SAIE-TE system. Data produced during calibrations were processed with dedicated software and stored in FITS[4] format files by DISCoS data archiver[5] (DISCoS, Detector Independent Science Console Subsystem).

4. THE CALIBRATION MEASUREMENTS

4.1. Detection Plane Calibration

The use of X-ray pencil beam at detection plane level calibration has allowed to study microstrip efficiency as a function of photon incidence position. Each strip constituting one of the four detector modules was irradiated with a constant intensity pencil beam in such a way that temporal data analysis could lead to the reconstruction of the photon incidence point.

Figure 4-a shows counts detected by two adjacent microstrips as a function of time and therefore as a function of beam position (see scale on top of the plot). The central region of the plot, which is related to inter-strip area, shows an efficiency decrease likely related to the structure of the electric field at the separation region between two nearby readout electrodes. The amount of lost counts in this inter-strip region is about 4% (integrated efficiency). Indeed, the weakening of field intensity in the inter-strip region and the presence of horizontal components for

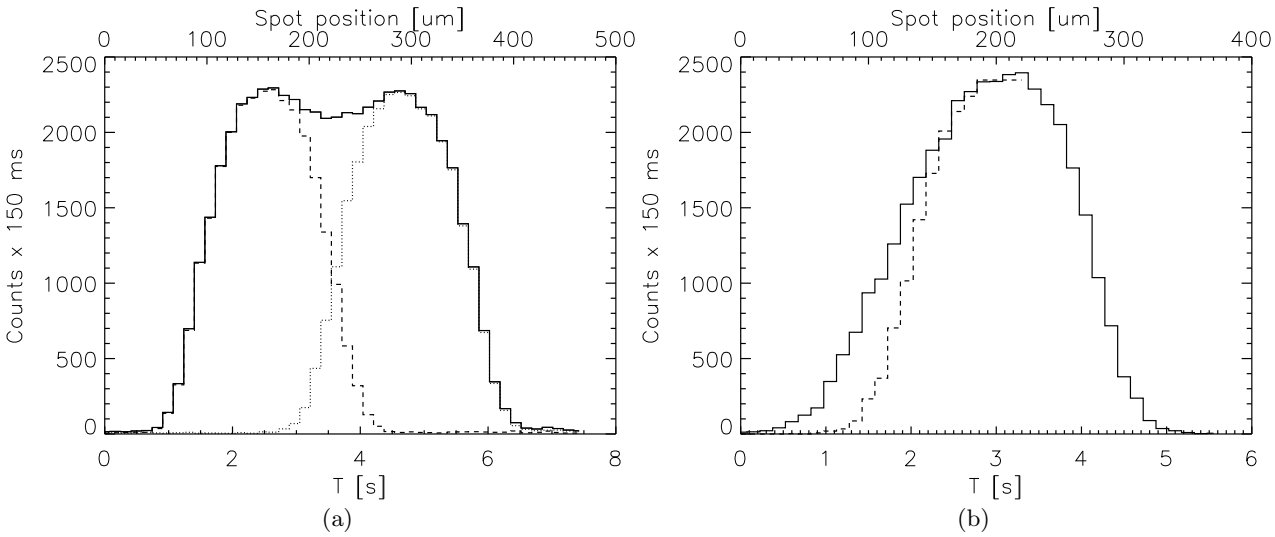

Figure 4. (a) Counts histogram for two contiguous microstrips (dashed line and dotted line) and total acquired counts (solid line). It stands to reason efficiency decreasing within interstrip region (spot position in 155 μm $\div$ 275 μm interval). (b) Counts acquired in function of time for first microstrip of silicon detector module (solid line). Dashed line represents ideal microstrip counts histogram.

electric field lines of force leads to two different phenomena which cause a decrease in efficiency. First, weak electric field involves increase of holes drift time, which leads to larger recombination probability. In this case part of the charge produced by photon can recombine and signal collected by read-out electronics could be below discriminator threshold. This effect is obviously larger for low energy photons, producing spectral distortion for certain radiation incidence angles. On the other side, non-vertical field lines involve charge-sharing between neighboring microstrips, creating two lower-energy signals which could be rejected by the discriminator. Our detected decrease in efficiency in the inter-strip regions will need to be taken into account in the construction of the SA response matrix and for the estimation of effective area. Indeed, this effect represents a non-monotonic variation of instrument spectral response as a function of photon direction (i.e., of source position).

Detection plane calibration has shown also border effects in electric field for microstrips situated at the edge of our silicon detector modules in spite of the presence of a guard-ring. In Figure 4-b solid line shows counts acquired as a function of time (i.e. beam position) by the first microstrip of a detection unit. In order to evaluate the deformation in sensible area of edge microstrips Fig. 4-b shows also a typical "light-curve" as acquired by other strips (dashed line). Border effects of electric field at detector edges lead to a broadening of the microstrip sensitive area, corresponding to about +10% in terms of detected counts with respect to other microstrips.

4.2. Integrated Experiment Calibration

This calibration was planned with the aim of studying the SA imaging response. Use of collimated X-ray beam and translational stage has allowed to emulate infinite distance point sources, being the detector irradiated homogeneously by a parallel X-ray beam. Owing to limited travel range of translational stage, each calibration run data set was obtained by merging two data sets acquired from two half-detectors. Calibrations were performed on all four detector modules with the X-ray beam approximately parallel to experiment axis, in order to simulate on-axis source, and with beam inclined $\sim$10° and $\sim$20° with respect to the SA axis for one detector unit only. Detected photons were energy selected between 27 keV and 45 keV to disentangle the intrinsic imaging properties from the distortions due to the detector image inhomogeneity caused by the XAA1.2 ASIC channels threshold dispersion, not yet equalized at the time of this calibration. Further filtering was performed by selecting counts integrated on each microstrip in a 6 seconds interval centered with respect to counts temporal distribution centroids. This filter optimized the signal with respect to the background induced by Compton scattering of

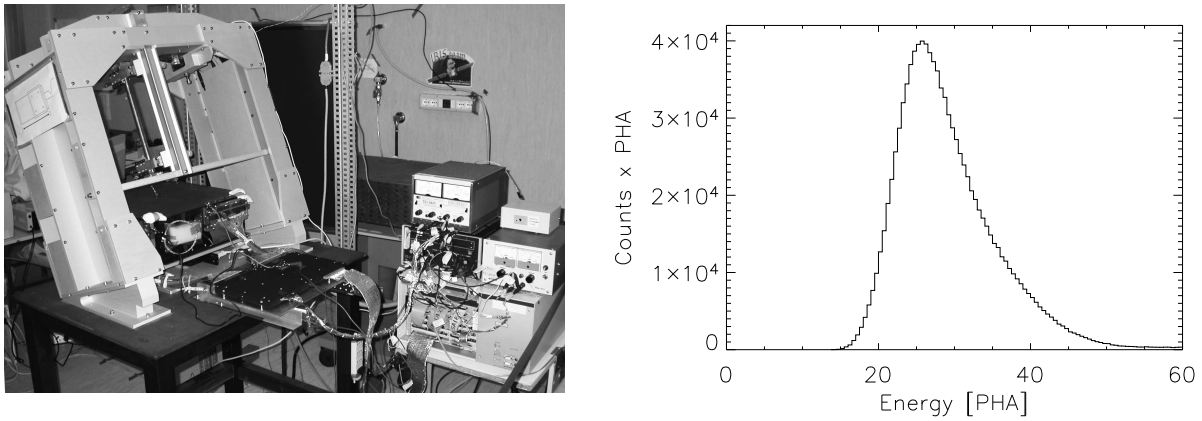

(a) (b)

Figure 5. (a) Mechanical setup used for integrated experiment calibration with the X-ray beam inclined of ∼20° with respect to SuperAGILE axis. (b) Spectrum acquired by one of four detector (D3) during calibrations.

incident photons in the aluminium plate supporting the detector. Each acquisition was carried out in order to obtain a signal-to-noise ratio greater than 900. Results from the detector images deconvolution process showed in Fig. 6 are summarized in Tab. 2.

Det.	**Reconstructed Source Pos. [Degrees]**	**Source Pos. Error [Degrees]**	**Total Source Counts (SC)**	**Image Peak Counts (PC)**	**PC/SC [%]**	**SNR**
D0	-0.4086	0.0005	1225307	1107387	90	1098
D0	9.64	0.01	1182390	974577	82	1078
D0	19.59	0.03	836255	630614	75	904
D1	-0.5081	0.0008	879755	756731	88	927
D2	0.5142	0.0009	764259	690397	90	863
D3	0.4146	0.0006	974529	918110	94	977

Table 2. Deconvolution results for detector images acquired with X-ray tube.

Variations in total source counts acquired by each detector are due to small differences between setup configurations and to dissimilarity in detector efficiencies (i.e., number of disabled channels). Sixth column in Tab. 2 shows the ratios between total counts and peak counts. The presence of percentages lower than 100% is due to the shape of instrument PSF, which produces variations in peak counts as a function of fine source position (within a sky pixel). Figure 7 shows PSF numerically simulated for an ideal point source at infinite distance, as a function of the fine off-axis position. The off-set step for each panel is 0.6 arcmin (0.1 sky pixel).

As far as the position reconstruction is concerned, which is showed in the second column of the table, on-axis acquisitions provide preliminary informations about single detector "optical" axis. Indeed considering that repeatability on SA orientation with respect to the X-ray beam is smaller than 0.1 arcmin, it is possible to use on-axis reconstructed positions as a measure of angular divergences between the four independent detector axis. Large signal-to-noise ratios have allowed to reach a very low statistical errors of position reconstruction. However, the real precision on position reconstruction in this measurements is connected to the knowledge of the instrument PSF. Our source position evaluation is obtained by a centroid calculation. This is of course based on the assumed knowledge of the instrument response (in this case, the shape of the deconvolved image). Variations

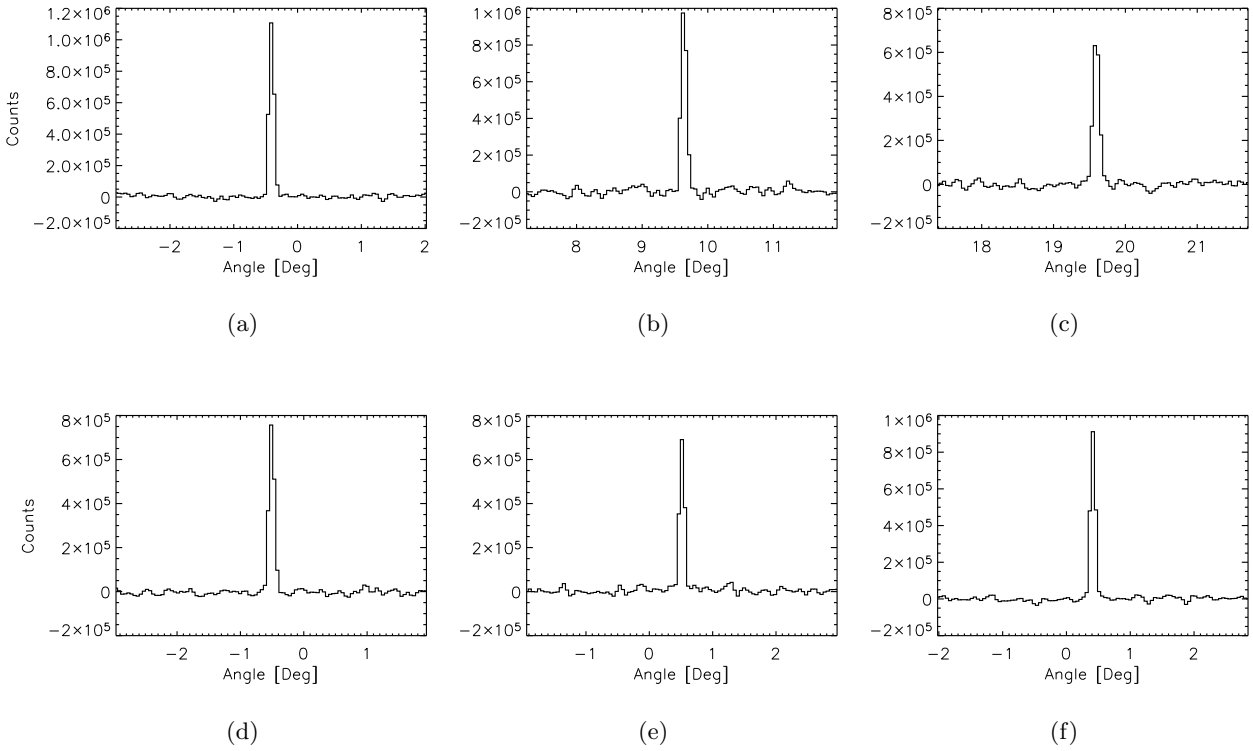

Figure 6. Sky images acquired with the X-ray tube by all of four SuperAGILE Detector Units. (a) D0 on-axis, (b) D0 off-axis 10 degrees, (c) D0 off-axis 20 degrees, (d) D1 on-axis, (e) D2 on-axis, (f) D3 on-axis.

between ideal and real PSFs could then lead to a wrong source reconstruction. Our current knowledge of the detailed geometry and physics of the SA experiment puts an upper limit on reconstructed position precision of about 0.3 arcmin for on-axis sources. Precision for off-axis sources gets slightly worse due to systematic effects like inclined penetration of X-ray, thickness of mask elements and deviations between ideal and real mask pattern*.

Thus, an exact estimate of the uncertainty of the position reconstruction in these images will require a deeper study of the expected PSF. In order to estimate real SuperAGILE PSF from calibration measurements a maximum likelihood iterative procedure was developed. The procedure makes a comparison between acquired image and simulated one, convolving source profile with the expected PSF for the source located in the same position. Each iteration modifies PSF in such a way that difference between real image and simulated one decreases, until this difference becomes equal or less than statistical fluctuations of acquired image. The procedure can be expressed as

$$PSF_{[n+1]} = PSF_{[n]} + \alpha \cdot (R - S_{[n]}) \tag{1}$$

where $PSF_{[n+1]}$ represents the PSF obtained with $n+1$ iterations, R is the real image, $S_{[n]}$ the simulated one after n iterations and α is a numeric coefficient which set the correction amplitude (typical values are $0.1 \leq \alpha \leq 0.2$). Procedure starting point ($PSF_{[0]}$) is a "triangular" PSF as is it showed in fifth panel of Fig. 7.

Results obtained with the likelihood procedure are showed in Fig. 8. Each panel displays acquired image (solid line) and correction that is necessary to apply to ideal instrument PSF in order to obtain the real image (dashed line). As expected correction to PSF becomes more significant with the off-axis angle.

*It is however worth reminding here that the in-flight SA source location accuracy will be most likely dominated by the uncertainty in the satellite attitude reconstruction, anticipated in the range between 1 and 2 arcminutes.

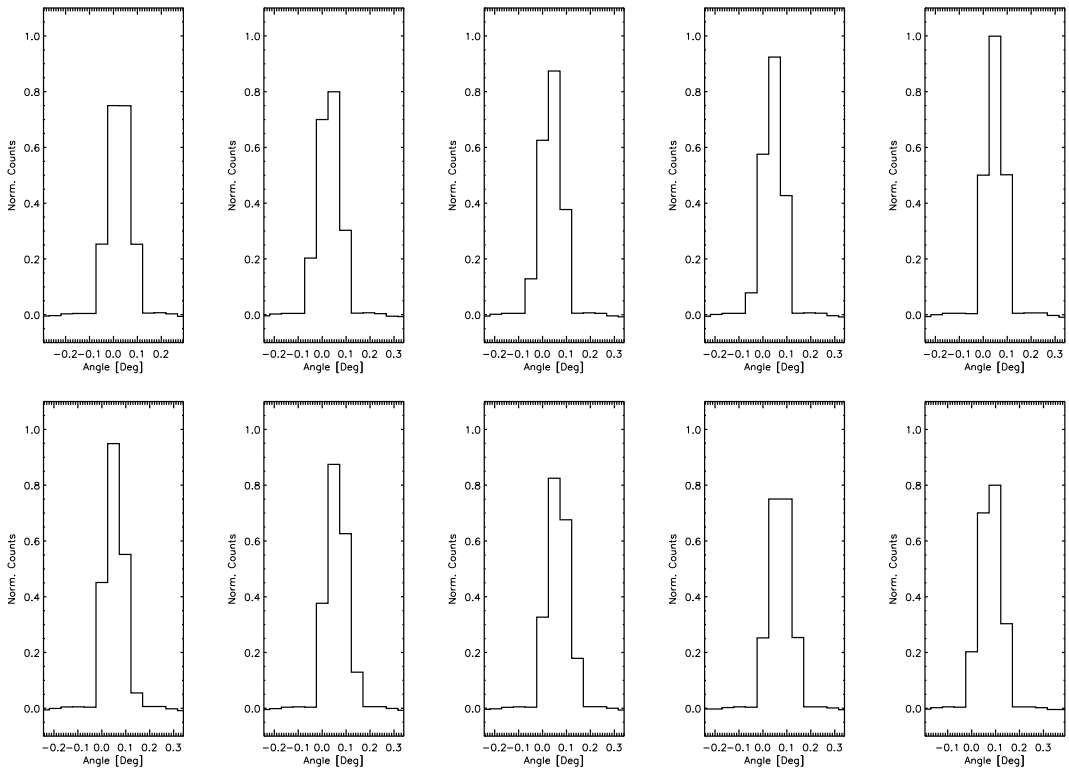

Figure 7. PSF numerically simulated for an ideal point source at infinite distance, as a function of the fine off-axis position, with an off-set step of 0.6 arcmin for each panel (0.1 sky pixel).

5. CONCLUSION

The on-ground calibrations of SuperAGILE have provided information about the instrument characteristics, regarding both detector and imaging response. The decrease in the quantum efficiency, produced by interference between the adjacent electric fields in the interstrip region, leads to an integrated interstrip efficiency defect of about 4% per strip. In terms of experiment performances, the total effect could be considered as a non-monotonic variation of instrument spectral response as a function of source position, and therefore it must be taken into account when developing the experiment response matrix. Due to the presence of the efficiency decrease in all the interstrips regions, the importance of this phenomenon is remarkably greater than the deformations in sensible area detected only at the edge of silicon detectors, which can be considered negligible. Concerning the imaging response of SuperAGILE, calibrations have showed sharp images response both for the on-axis acquisition and for source positioned 10° and 20° off-axis. Together with the calibrations obtained with radioactive sources at larger off-axis angle,[2] this confirms that the entire wide Field Of View of SA is suitable in the detection and localization of astrophysical sources. The emulation of a point source situated at infinite distance with small angular divergence has also allowed to extract the instrumental PSF from the detected images. This information will be complemented with the calibration performed using omnidirectional radioactive sources at finite distance, in order to build an accurate modelization of the instrument imaging response.

ACKNOWLEDGMENTS

The SuperAGILE Team is grateful to Pietro Ubertini and to all the IBIS Team for making their clean room facility available for SA testing and calibrations.
We want to thank M. Trifoglio, A. Bulgarelli and F. Gianotti for providing and continuously supporting the DISCoS system for SA.

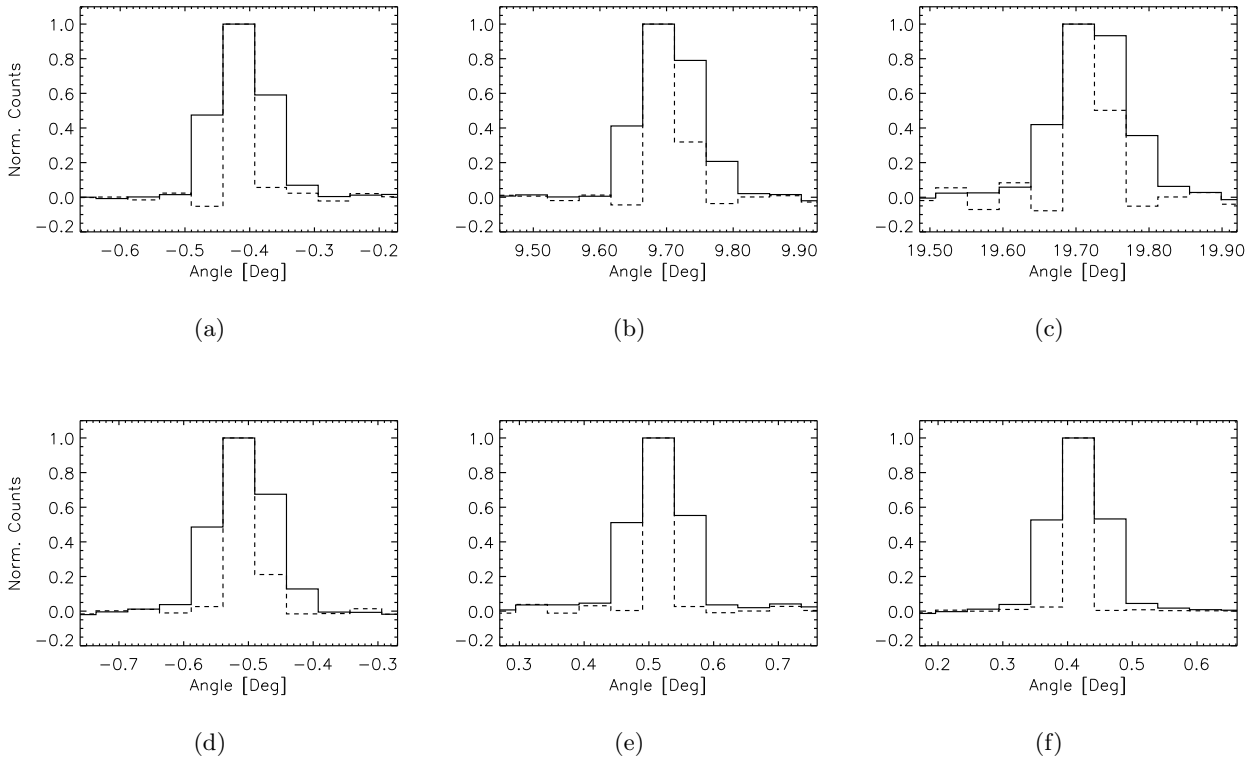

Figure 8. Acquired images (solid lines) and correction to ideal PSFs (dashed lines) obtained with the likelihood procedure for all of four SuperAGILE detector units. (a) D0 on-axis, (b) D0 off-axis 10 degrees, (c) D0 off-axis 20 degrees, (d) D1 on-axis, (e) D2 on-axis, (f) D3 on-axis.

REFERENCES

1. P. Soffitta et al., "SuperAGILE at launch", in *Proceedings of the SPIE*, **6266**, 2006.
2. I. Donnarumma et al., "The On-Ground Calibrations of SuperAGILE: II. Finite Distance Radioactive Sources", in *Proceedings of the SPIE*, **6266**, 2006.
3. L. Pacciani et al., "Instrumentation for Ground Test of SuperAGILE Detectors and Front-End Electronics", in *Proceedings of the SPIE*, **5488**, pp. 719–730, 2004.
4. R. J. Hanisch et al., "Definition of the Flexible Image Transport System (FITS)", *Astron. Astrophys.* **376**, pp. 359–380, Sept. 2001.
5. F. Gianotti et al., "DISCoS—Detector-Independent Software for On-Ground Testing and Calibration of Scientific Payloads Using the ESA Packet Telemetry and Telecommand Standards", in *ASP Conf. Ser. 238: Astronomical Data Analysis Software and Systems X*, p. 245, 2001.